Current Opinion in Solid State and Materials Science 16 (2012) 216–226

Contents lists available at SciVerse ScienceDirect

Current Opinion in Solid State and Materials Science

journal homepage: www.elsevier.com/locate/cossms

Nanoscale characterization of emergent phenomena in multiferroics

Q. He [a,*], E. Arenholz [a], A. Scholl [a], Y.-H. Chu [b,c], R. Ramesh [b,d]

[a] Advanced Light Source, Lawrence Berkeley National Laboratory, Berkeley, CA 94720, USA
[b] Department of Physics, University of California Berkeley, CA 94720, USA
[c] Department of Materials Science and Engineering, National Chiao Tung University, Hsinchu 30010, Taiwan
[d] Department of Materials Science and Engineering, University of California Berkeley, CA 94720, USA

ARTICLE INFO

Article history:
Available online 5 April 2012

Keywords:
Multiferroics
Magnetoelectrics
Photoemission electron microscope

ABSTRACT

Multiferroics exhibit intriguing physical properties and in turn promise new device applications — as a result of the coupling between their order parameters. In this review article, we introduce photoemission electron microscopy (PEEM) as a powerful tool to study multiferroicity with the capability of probing the charge, spin and orbital states of a material simultaneously with nanoscale spatial resolution and element sensitivity. Several systematical studies of ferroelectricity, antiferromagnetism, and multiferroicity using PEEM are discussed. In the end, we outline several challenges remaining in multiferroic research, and how PEEM can be employed as an important characterization tool providing critical information to understand the emergent phenomena in multiferroics.

Published by Elsevier Ltd.

1. Introduction

Ferroics are materials with a spontaneous, reversible ordering. The best known are ferromagnets, where the ordering of spins can be reversed by a magnetic field. Similarly, in ferroelectrics, aligned electric-dipoles can be reversed by an electric field and in ferroelastics, strain alignment can be altered by a stress field. Ferroics have been of great interest both for their fundamental physics and for their potential technological applications. In the last decade there has been a significant amount of research focused on magnetoelectric multiferroics, i.e. the phenomenon of inducing magnetic or electric polarization by applying an external electric or magnetic field [1,2]. These systems exhibit unusual physical properties — which in turn promise new device applications — as a result of the coupling between their order parameters [3–5]. The correlation of order parameters required of ferroic materials to be classified as multiferroic is shown schematically in Fig. 1 [6]. Only a small subgroup of magnetically and electrically polarizable materials are either ferromagnetic or ferroelectric and fewer still simultaneously exhibit both order parameters. In these materials, however, there is the possibility that electric fields cannot only reorient the polarization but also control magnetization; similarly, a magnetic field can change the electric polarization. These functionalities offer intriguing degrees of freedom and we refer to such materials as magnetoelectrics. Current interests focus more on materials that combine ferroelectricity with ferromagnetism or, more loosely, with any kind of magnetism, i.e. ferri- and antiferromagnetism are also considered. The terminology is often extended to include composite heterostructures, such as ferroelectrics interlayered with magnetic materials and ferromagnets embedded in ferroelectric matrix [5]. The promise of coupling magnetic and electronic order parameters and the potential to manipulate one through the other has captured the attention of researchers worldwide. In terms of applications, the prospect of electric-field control of magnetism is particularly exciting, as it could lead to smaller, more energy-efficient devices.

The key to realize the application of multiferroics into real devices depends on the basic understanding of the material systems. Advanced characterization techniques, such as X-ray diffraction (XRD), Raman spectroscopy, second-harmonic generation (SHG), neutron scattering, and transmission electron microscopy (TEM), have been applied and served in the study of multiferroics to extract critical information of various multiferroics. XRD has been widely employed to characterize the crystal structure of the materials, as well as probing the structural phase transitions. Recently, giant magneto-elastic coupling in multiferroic manganites has been carefully observed with XRD and other diffraction methods. Temperature-dependent XRD reciprocal space mapping also has been used to find the concurrent transition of ferroelectric and magnetic ordering near room temperature [7–9]. Neutron scattering, an excellent probe of both structure and magnetic order, has been applied to study the magnetic structure and the coupling between the ferroelectric and antiferromagnetic directions for single crystals of multiferroic $BiFeO_3$ [10]. Sensitive to symmetry breaking, SHG is a powerful tool to study ferroelectric and magnetic orders in multiferroics, especially at surfaces and buried interfaces. Researchers have observed a giant coupling of SHG to the sponta-

* Corresponding author. Tel.: +1 510 642 2347; fax: +1 510 643 5792.
E-mail address: qhe@lbl.gov (Q. He).

1359-0286/$ - see front matter Published by Elsevier Ltd.
http://dx.doi.org/10.1016/j.cossms.2012.03.006

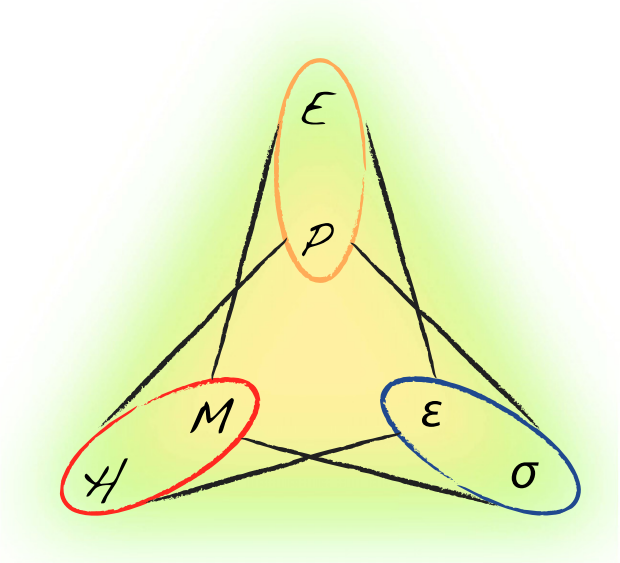

Fig. 1. Interactions in multiferroics. The well-established primary ferroic orderings, ferroelectricity (P), ferromagnetism (M), and ferroelasticity (ε), can be switched by their conjugate electric (E), magnetic (H), and stress (σ) fields, respectively. Cross coupling allows those ferroic orderings to also be tuned by fields other than their conjugates; in magnetoelectric multiferroics, for example, an electric field can modify magnetism.

neous polarization in compounds with magnetically-driven ferroelectricity, such as $TbMn_2O_5$ [11]. Utilizing spin waves in multiferroics is one pathway to low-power high frequency application, especially in the terahertz range. Recently, electric-field controllable magnonics is realized in multiferroic $BiFeO_3$ at room temperature by probing with Raman spectroscopy [12]. However, ferroics typically show complex domain structures, most of these techniques do not offer the spatial resolution to probe multiferrocity in nanoscale region. This is crucial, especially when we want to take full advantages of the coupling between order parameters in magnetoelectric multiferroics for device applications [13,14].

Domain formation occurs to minimize the total free energy of a system. In a ferromagnet, the single domain state will minimize the exchange interaction energy. For example, the energetically most favorable magnetic state of a thin film is to align all the spins parallel in the film plane. However, the magnetic stray field associated with this configuration around any finite sample leads to a huge the magnetostatic energy. As a consequence, closure domains form and reduce the stray field but increase the exchange energy at the domain walls and anisotropy energy for the spins oriented away from their magnetic easy axis. This domain configuration is the most common in magnetic materials [15]. Similarly, in the case of ferroelectric materials, the competition of several energy terms, i.e. dipole–dipole interaction energy and anisotropy energy, lead to a complex domain configuration in the system [16]. Domain structures in ferromagnets and ferroelectrics can be studied by magnetic force microscopy and piezo-response force microscopy (PFM), respectively. However, in order to study multiferroicity, a technique, which can simultaneously study the domain structures of different order parameters is highly desirable. Second harmonic generation has been demonstrated to be a powerful tool to study multiferroic single crystals, which typically have large domains [17]. The characterization down to nano-size region remains elusive. In this review article, we will show that photoemission electron microscopy (PEEM) [18] using synchrotron radiation for excitation provides a powerful tool to study multiferroicity with nano-scale spatial resolution.

2. Physics of photoemission electron microscopy

PEEM can employ soft X-rays generated at a synchrotron for excitation of electrons from the sample of interest using the photoelectric effect. The spatial distribution of the electrons is then observed. In the X-ray absorption process, electrons are excited from core levels to unoccupied valence states, leaving empty core states. The decay of these core holes generates Auger electrons and fluorescence photons. The primary Auger electrons lose their energy through inelastic scattering processes creating an electron cascade. The total number of the low-energy electrons that escape from the sample into vacuum is proportional to the probability of creating an Auger electron and hence the X-ray absorption probability. Mapping the spatial distribution of the secondary electrons using electron optics in a photoemission electron microscope therefore images directly the spatial variation of the X-ray absorption at the chosen photon energy. Since the scattering cross section of electrons in solids is large, the emitted electrons originated in the top 2–5 nm of the sample, which makes PEEM a surface sensitive technique [19]. The secondary electrons are accelerated by a voltage of between 15 kV and 20 kV from the sample to an electro-magnetic lens system and generate a magnified image on a charge-coupled device (CCD). Affected most by the chromatic and spherical aberrations, – i.e. the energy and angular distribution of the electrons – PEEM typically provides a spatial resolution of tens of nanometers using soft X-rays [18]. With the implementation of aberration correction, a spatial resolution of potentially better than 5 nm is expected.

2.1. Advantages of PEEM

Using soft X-ray generated by a bending magnet or insertion device at a synchrotron facility has many advantages. The photon beam has orders of magnitude higher brightness than standard laboratory sources, superior monochromaticity (energy resolution better than 0.01 eV), wide tunable X-ray energy range, as well as full polarization control (left and right circular as well as linear with variable orientation. Within the soft X-ray region (100–2000 eV), many elements show strong absorption edges that can be used for element-selective imaging [20]. By tuning the energy of the incident X-rays to an absorption edge, PEEM allows studying the spatial distribution of elements in a material or different layers in a multilayered structure in case elements are distributed suitably. For example, in a $Co/BiFeO_3$ bi-layer, the Co and Fe electronic and magnetic structure can be studied separately. X-ray absorption spectra provide important information on valence and spin states, orbital orientations, as well as crystal field effects to the atoms of interests.

2.2. dichroism

Taking advantage of the fact that X-ray absorption depends sensitively on the polarization of the beam allows a detailed characterization of the sample using linear as well as circular dichroism. Dichroism is defined as the polarization dependent absorption of light. Three kinds of X-ray dichroism – X-ray natural linear dichroism (XNLD), X-ray magnetic circular dichroism (XMCD), and X-ray magnetic linear dichroism (XMLD) – are particularly interesting in the study of ferroic/multiferroic materials [21]. XNLD rises from a charge distribution anisotropy where the spins are not aligned, i.e. in ferroelectrics. The largest XNLD effect can be measured as the absorption difference between the E vector points parallel and perpendicular to the direction of the maximum density of the charge probed by "search light effect" [21]. XMCD arises from directional spin alignment, i.e. in ferro- or ferrimagnets,

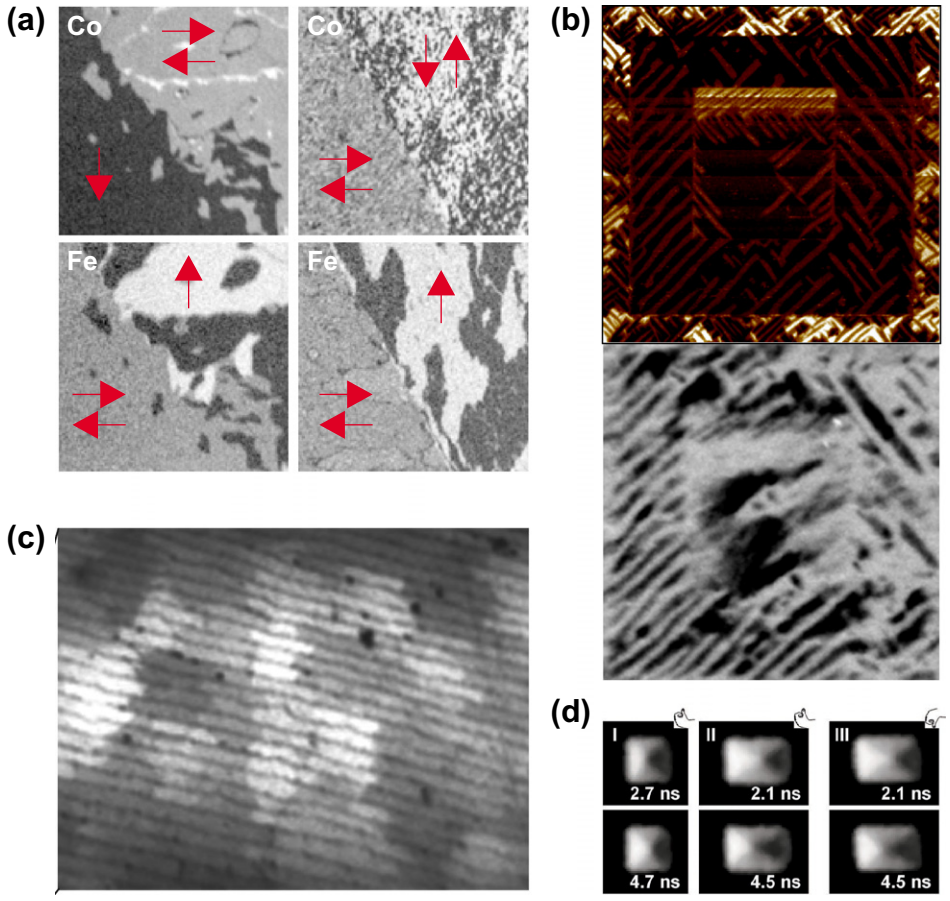

Fig. 2. Imaging magnetic and structural domains using PEEM. (a) Co and Fe magnetic domains imaged using XMCD at the Co and Fe L_3 edges in Co(2 nm)/NiO/Fe(15 ML)/Ag (001) heterostructure with different NiO layer thicknesses (1.8 nm in left panel, 2.4 nm in right panel. (b) Magnetic domains in CoFe and ferroelectric domains in $BiFeO_3$ in Pt(1.5 nm)/CoFe(2.5 nm)/$BiFeO_3$(100 nm)/$SrTiO_3$ (001) heterostructure. XMCD-PEEM image (lower) obtained at the Co absorption edge shows the same domain pattern as the IP-PFM image (upper) taken at the same area. (c) XLD-PEEM image obtained at the O K edge, which illustrates the different orientations of the carbonate crystal *c*-axis. The contrast level in this image scales with the angle difference between the X-ray polarization vector *E* and carbonate crystal *c*-axis. (d) XMCD-PEEM images obtained at the Co L_3 edges of rectangular pattern with different dimensions: Pattern I, $1 \times 1\ \mu m^2$; Patterns II and III, $1.5 \times 1\ \mu m^2$. The images on top and bottom were taken at the specified delay after a field pulse was applied to the patterns in a pump–probe setup. The vortex dynamics can be resolved using this approach.

which can be used to measure the size and direction of magnetic moments with circularly polarized X-rays. This effect is usually seen at the resonance positions of the magnetic elements, i.e. the $L_{2,3}$ edges of the 3*d* transition metals. XMLD arises from axial spin alignment, i.e. in ferro-, ferri- or antiferromagnets, which is used in the study of antiferromagnetism with linearly polarized X-rays. Unlike ferro- or ferrimagnets, antiferromagnets do not have any net magnetic moment. However, the axial spin alignment gives rise to a charge distribution anisotropy through spin–orbital coupling, which results in a large XMLD effect typically seen in the absorption fine structure of the resonance peaks in transition metal oxides. Combining X-ray circular and linear dichroism measurements and analysis, PEEM imaging has also been widely applied in the study of (anti-)ferromagnetic and ferroelectric domain structure (Fig. 2a and b [22,23]) and crystal orientations (Fig. 2c [24]) in both magnetic and non-magnetic nanostructures. By synchronizing the applied field or pump laser with the synchrotron electron bunches, researchers have also demonstrated dynamic imaging of PEEM with a pump–probe measurement design (Fig. 2d [25]).

With the capability of probing the charge, spin and orbital states of a material simultaneously with nanoscale spatial resolution and element sensitivity, PEEM is a very powerful tool to study the interplay and coupling between multiple order parameters in multiferroics. We will present several systematical studies of ferroelectricity, antiferromagnetism, and multiferroicity using PEEM in the following sections.

3. Ferroelectricity

Ferroelectric oxides exhibit a spontaneous, stable, and switchable electric polarization that is due to atomic displacements of positive transition metal ions and negative oxygen ions in opposite directions, which reduces the symmetry of the crystal lattice [26]. The ferroelectric $PbZr_{0.2}Ti_{0.8}O_3$ (PZT) for example has a tetragonal perovskite structure where the Ti^{4+} and Zr^{4+} ions occupy the centers of a cube, the Pb^{2+} ions are located at the corners and the O^{2-} ions are centered on each face of the undistorted lattice. In the ferroelectric phase the Ti^{4+} and Zr^{4+} ions are displaced leading to a net electric dipole polarization [27]. To shed light on the impact of ferroelectric order on the electronic and atomic structure of ferroelectric PZT films deposited on $SrRuO_3$ (SRO) electrodes which in turn were grown on (100)-oriented $SrTiO_3$ substrates, soft X-ray absorption (XA) spectroscopy was employed as well as PEEM [28].

Fig. 3a shows Ti $L_{3,2}$ XA spectra obtained from epitaxial PZT. It reflects electric dipole transitions from a Ti^{4+} d^0 ground state configuration to $2p^5\ 3d^1$ final states. The 2*p* spin–orbit interaction splits the spectrum into $2p_{3/2}$ (L_3) and $2p_{1/2}$ (L_2) features which are further split by crystal field interaction, i.e., the electrostatic potential due to the neighboring lattice sites acting on the 3*d* orbitals. In octahedral site symmetry the *e* orbitals of Ti^{4+} point toward the oxygen ligands, while the t_2 orbitals point in between them, resulting in a lower energy for the latter. Lowering to tetragonal

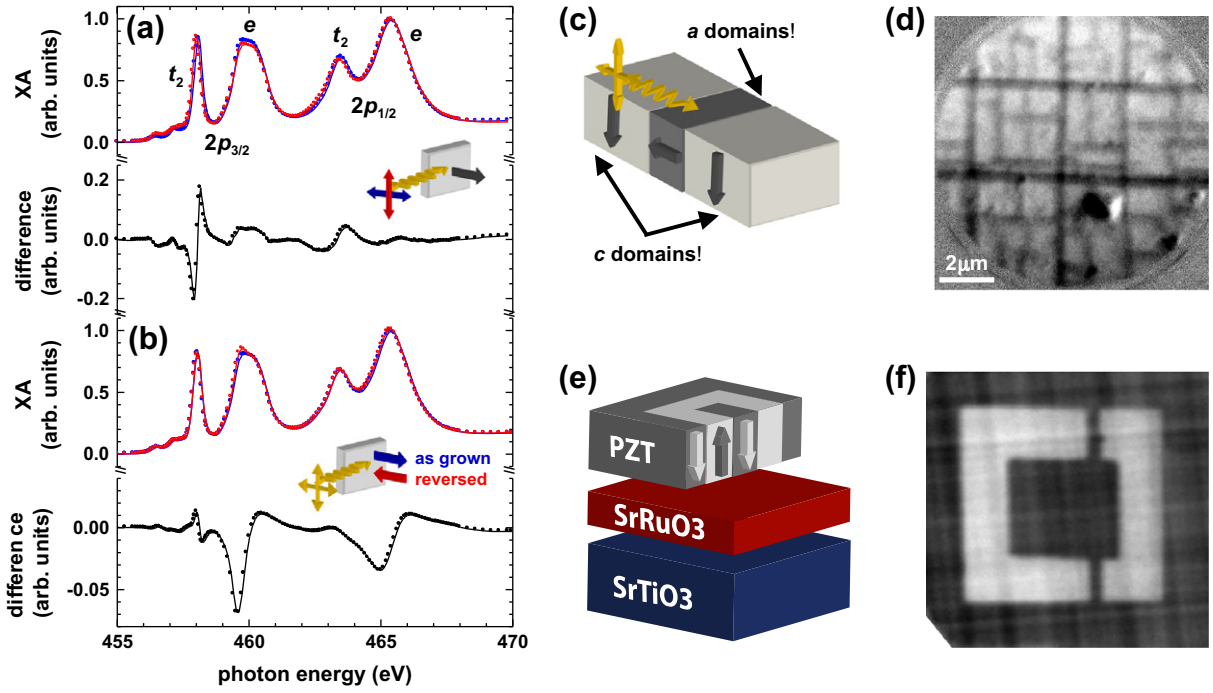

Fig. 3. Experimental Ti $L_{3,2}$ XA and difference spectra of a PZT thin. (a) Spectra obtained with the X-ray polarization aligned in the surface plane and pointing out of the surface plane are indicated by solid (blue) and open (red) symbols, respectively in the top panel while their difference spectrum is indicated in black in the bottom panel. (b) Polarization-averaged Ti $L_{3,2}$ XA spectrum obtained with the ferroelectric polarization pointing away from and towards the bottom electrode is shown in solid (blue) symbols and the spectrum resulting with the polarization pointing toward the electrode is shown by open (red). The difference spectrum is shown in black. Insets depict experimental geometries. The ferroelectric polarization collinear with the surface normal is indicated by a one-ended arrow, the incident X-ray beam by a yellow wave and the X-ray polarization by double-ended arrows. (c and d) Schematic and PEEM image of *a* domains (dark gray lines) and *c* domains (light gray areas) imaged using soft X-rays. (e and f) Schematic and PEEM image of as-grown domains (dark gray areas) and electrically switched domains (light gray areas).

symmetry splits the $t_2(O)$ states into $d(xy)$ and $d(xz, yz)$ and the $e(O)$ states into $d(x^2 - y^2)$ and $d(z^2)$. The four main features in the Ti $L_{3,2}$ spectra are labeled accordingly in Fig. 3a. This anisotropy in charge distribution around the Ti^{4+} absorbers induces a difference between XA spectra taken with polarization along the *z* and *x*, *y* directions, i.e., parallel and perpendicular to the surface normal [28]. We observe a ±20% difference in the photon energy range of the $2p_{3/2}3d$ (t_2) peak shown in Fig. 3a. Smaller but still easily detectable intensity differences are found at higher photon energies.

To further determine the impact of the ferroelectric polarization on the XA spectra, it was reversed from pointing towards the sample surface in the as grown configuration to point towards the bottom electrode in a 30 μm × 30 μm area using an applied voltage between the tip and the sample in PFM. Fig. 3b shows a comparison of the XA results of PZT/SRO obtained from sample areas with opposite ferroelectric polarization. The data are the average of XA spectra obtained with the X-ray polarization aligned in the surface plane and perpendicular to it. Fig. 3b shows the difference spectrum as well.

It is at first sight rather surprising that the PZT measurements reveal two distinct difference spectra, i.e., a first difference spectrum between XA spectra obtained with the X-ray polarization parallel and perpendicular to the ferroelectric polarization (Fig. 3a) caused by the tetragonal distortion of the lattice and a distinct second difference spectrum between XA spectra with the ferroelectric polarization pointing toward the bottom electrode and away from it (Fig. 3b). Since in tetragonal symmetry there can be only one linear dichroism spectrum, structural differences must be associated with the reversal of the ferroelectric polarization.

To confirm the presence of the structural changes with polarization reversal as cause for the difference in Ti^{4+} XA spectra, the polarization averaged XA spectra of PZT/SRO systems with varying PZT layer thickness resulting in lattice constants $c = 0.414$ and 0.416 nm as determined by X-ray diffraction have been compared. The samples are in the as-grown state—i.e., the ferroelectric polarization points away from the bottom electrode. It is noted that the sample with $c = 0.416$ nm—i.e., the sample with elongated *c* axis—exhibits a difference spectrum with the same spectral shape as shown in Fig. 3b. This clearly confirms the finding of the structural changes associated with the reversal of the ferroelectric polarization in PZT.

Using these results the dependence of X-ray absorption on the orientation of the ferroelectric polarization can now be used to image ferroelectric domains using PEEM. Tetragonal PZT thin films on SRO show a domain structure consisting of alternating *c* domains present as extended areas with the tetragonal axis perpendicular to the film-substrate interface, intercepted by line-like *a* domains (90° domains) with the *c* axis of the tetragonal film along either (1 0 0) or (0 1 0) directions of the substrate (Fig. 3c) [29]. The formation of these domain structures in ferroelectric films is a mechanism of strain energy relaxation. Fig. 3d shows the *c* and *a* domain structure of a PZT/SRO sample obtained at the Ti $L_{3,2}$ edges with linear polarized soft X-rays. Similarly, artificially written domains that created by inducing 180° ferroelectric switching with PFM tips (Fig. 3e) can also be imaged by PEEM (Fig. 3f) utilizing the same effect.

These results show that polarization dependent X-ray absorption spectroscopy and microscopy are powerful tools for the study of ferroelectric order.

4. Antiferromagnetism

PEEM is also a unique tool for the study of antiferromagnetic domains in thin films and single crystals on the nanometer scale. Due to the lack of observable net magnetization, the techniques

that can be used to study the antiferromagnetic domain structures are limited. Although the antiferromagnetic domain structure in bulk crystal has been determined with neutron diffraction topography (~70 μm) and X-ray diffraction topography (1–2 μm) [30], little was known about the antiferromagnetic domain structure in thin films due to the small domain size in those systems. The combination of X-ray magnetic linear dichroism – i.e. the dependence of X-ray absorption on the relative orientation of spin axis and X-ray linear polarization vector – with photoemission electron microscopy provides a unique tool for studying antiferromagnetic domains in the near-surface region of solids.

PEEM imaging of antiferromagnetic domain structures was demonstrated on $LaFeO_3$ thin films epitaxially grown on $SrRuO_3$ [31]. Two (100) crystals were joined macroscopically at (110) and (010) faces, leading to a 45° rotation of the lattice around the surface normal. The experiments made use of the large X-ray magnetic linear dichroism (XMLD) effect previously observed in α-Fe_2O_3 [32]. In both α-Fe_2O_3 and $LaFeO_3$, the Fe^{3+} ion has a $3d^5$, high-spin $S = 5/2$ ground state and an approximately octahedral environment. For octahedral symmetry, there is no conventional linear dichroism arising directly from the charge asymmetry of the orbitals as observed in the previous case (PZT). The XMLD observed in this system is the difference in cross section for light polarized perpendicular or parallel to the magnetic moment with the dependence given by [33,34]

$$I(\theta, T) = a + b(3\cos^2\theta - 1)\langle M^2\rangle_T \quad (1)$$

where the first term is a constant and θ is the angle between the E vector of the polarized X-ray and the preferential orientation of the antiferromagnetic axis A of the material. The vanishing of the temperature-dependent, second term above Neel temperature is generally taken as proof of its magnetic origin.

This XMLD effect is illustrated in Fig. 4a. The Fe^{3+} L-edge X-ray absorption spectra for $LaFeO_3$ were taken with the E vector along and perpendicular to the sample normal. A pronounced difference can be seen between these two spectra. In particular, peak A at 721.5 eV is larger than peak B at 723.2 eV (Fig. 4a inset) for E parallel to A and smaller for E perpendicular to A.

AFM domains can be directly observed by combining XMLD spectroscopy with PEEM microscopy; that is, by dividing a PEEM image acquired at 723.2 eV (peak B) by one obtained at 721.5 eV (peak A). The resultant image (Fig. 4b) was recorded across the bicrystal junction (crystal orientation is indicated by arrows) and reveals striking AFM domains on the right side of the junction and a uniform gray shade on the left side. The strong magnetic contrast on the right side arises from magnetic domains with an in-plane projection of A parallel (white) and perpendicular (black) to the horizontal E vector. On the left side, the domains cannot be distinguished because E has an equal 45° projection onto the two orientations of A.

In a collection of XMLD images (Fig. 4c) obtained at different temperatures between 290 and 550 K, the image contrast is strongly reduced at elevated temperatures and it is completely reversible upon cooling to room temperature, showing a clear temperature dependence of the XMLD effect. The quantitative XMLD image contrast is also plotted (Fig. 4d), measured for two temperature cycles. According to Eq. (1), the XMLD contrast is a measure of the square of the AFM moment $\langle M^2\rangle_T$. We have fitted the data in Fig. 4d with the shown solid line, using the exact expression for $\langle M^2\rangle_T$ in terms of $\langle M\rangle_T$ [35]. $\langle M\rangle_T$ has been approximated following mean field theory with $S = 5/2$. Data and fit are normalized to 1 at 0 K. From the fit, we obtain the Neel temperature (T_N) = 670 ± 10 K for the thin film. The temperature dependence shown in Fig. 4d clearly establishes the AFM origin of the image contrast and indicates that crystallographic distortions of the octahedral Fe environment make only a negligible contribution.

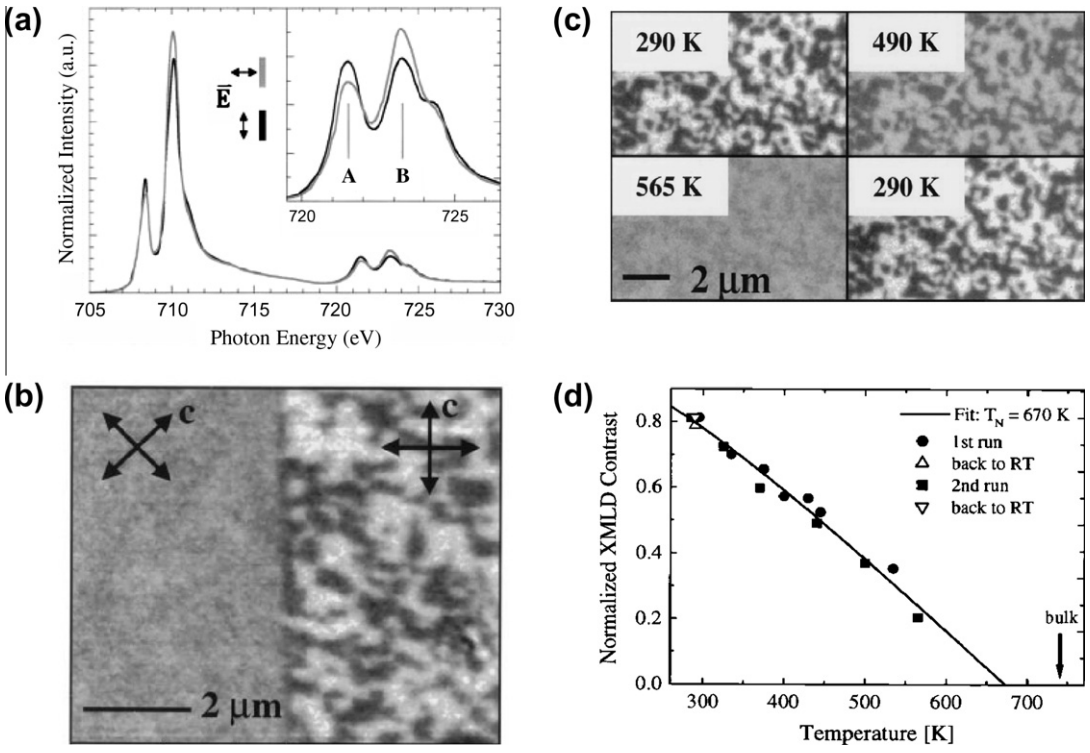

Fig. 4. PEEM images of the antiferromagnetic domain structures in $LaFeO_3$ thin films. (a) Fe L-edge XMLD spectra for a $LaFeO_3$ film grown on $SrTiO_3$ substrates, measured with the E vector parallel (in black) and perpendicular (in gray) to the sample surface. (b) XMLD-PEEM image obtained by division of images taken at photon energies 723.2 eV (peak B) and 721.5 eV (peak A). Arrows indicate the orientation of the antiferromagnetic easy axes. The X-ray polarization E lies in the film plane. (c) XMLD-PEEM images at various temperatures. (d) Temperature dependence of quantitative XMLD image contrast. The data and fit are normalized to 1 at 0 K.

5. Multiferroism

Multiferroism in materials can be achieved through different pathways [36]. For example, a multiferroic can be a material in which ferroelectricity and magnetism have different sources and appear largely independent of one another. This can be created by site-engineering the functionality in model systems like perovskites (ABO_3) where one can make use of the stereo-chemical activity of an A-site cation with a lone pair (i.e., 6 s electrons in Bi or Pb) to induce a structural distortion and ferroelectricity while inducing magnetism with the B-site cation. One of the most widely studied single-phase multiferroics in this case is the antiferromagnetic, ferroelectric $BiFeO_3$ (BFO) [37]. Another pathway to create a multiferroic is through geometrically driven effects where long-range dipole–dipole interactions and anion rotations drive the system towards a stable ferroelectric state, such as $YMnO_3$ [38]. Furthermore, there can also be charge ordering driven multiferroics where non-centrosymmetric charge ordering arrangements result in ferroelectricity, one good example is $LuFe_2O_4$ [39]. There are multiferroics in which magnetism causes ferroelectricity—suggesting a strong coupling between the two order parameters. The prototypical examples of this sort of behavior are $TbMnO_3$ [40] and $TbMn_2O_5$ [41] where ferroelectricity is induced by the formation of a symmetry-lowering magnetic ground state that lacks inversion symmetry.

A model multiferroic system to demonstrate the electric and magnetic correlation is BFO. It is a room temperature, single-phase, multiferroic material with a high ferroelectric Curie temperature (~1103 K) and a high antiferromagnetic Néel temperature (~643 K) [42]. The structure of BFO is characterized by two distorted perovskite unit cells (a_r = 3.96 Å, α_r = 0.6°) connected along their body diagonal, denoted as the pseudocubic ⟨1 1 1⟩ (Fig. 5a), to build the rhombohedral unit cell [43]. The ferroelectric state is realized by a large displacement of the Bi ions relative to the FeO_6 octahedra. The ferroelectric polarization in BFO, therefore, can be aligned along the four cube diagonals ⟨1 1 1⟩. The direction of the polarization can be changed by ferroelectric (180°) and ferroelastic switching events (71° and 109°) [44]. The antiferromagnetic ordering of BFO is G-type, i.e. the Fe magnetic moments are aligned ferromagnetically within pseudocubic (1 1 1) planes (green planes in Fig. 5a) and antiferromagnetically between adjacent (1 1 1) planes. The preferred orientation of the antiferromagnetically aligned spins is in the (1 1 1) plane perpendicular to the ferroelectric polarization direction, with six equivalent easy axes within that plane [45]. The rotation of the ferroelectric polarizations always results in a re-orientation of the antiferromagnetic easy plane to preserve the orthogonality relation between them. The antiferromagnetism is therefore coupled to the ferroelectric polarization. Recent studies of BFO thin films have shown the existence of a large ferroelectric polarization, as well as a small net magnetization of the Dzyaloshinskii-Moriya type resulting from a canting of the antiferromagnetic sublattice [46]. It has also been noted that BFO films show a very complicated domain structure, which needs to be understood for eventual device integration.

Recently, the coupling between ferroelectricity and antiferromagnetism in BFO thin films was demonstrated by a combination of PFM and PEEM, which is attributed to the coupling of both antiferromagnetic and ferroelectric domains to the underlying domain switching events [22,47]. The ferroelectric domain structure of BFO thin films are frequently characterized by PFM.[22,44] In PFM, domains with up- and down-polarizations give rise to opposite contrast in out-of-plane (OOP)-PFM images. In-plane components of the polarization produce a torque on the AFM cantilever and create contrast in the in-plane (IP)-PFM images. Furthermore, domains with polarization vectors along the scanning cantilever's long axis do not give rise to any IP-PFM contrast. However, domains with the polarization pointing to one side of the cantilever's long axis should produce an opposite tone as compared with domains having polarization pointing to the opposite side of the cantilever. This is caused by the antiphase IP-piezoresponse (PR) signals produced by these domains. By combining the OOP-PFM and IP-PFM images, therefore, we can identify the polarization direction of each domain [44]. Fig. 5b shows an IP-PFM image of a BFO film grown on a (0 0 1) $SrTiO_3$ (STO) substrate. The three contrast levels observed in the IP-PFM images acquired along the two orthogonal ⟨1 1 0⟩ directions, together with the uniform OOP-PFM contrast

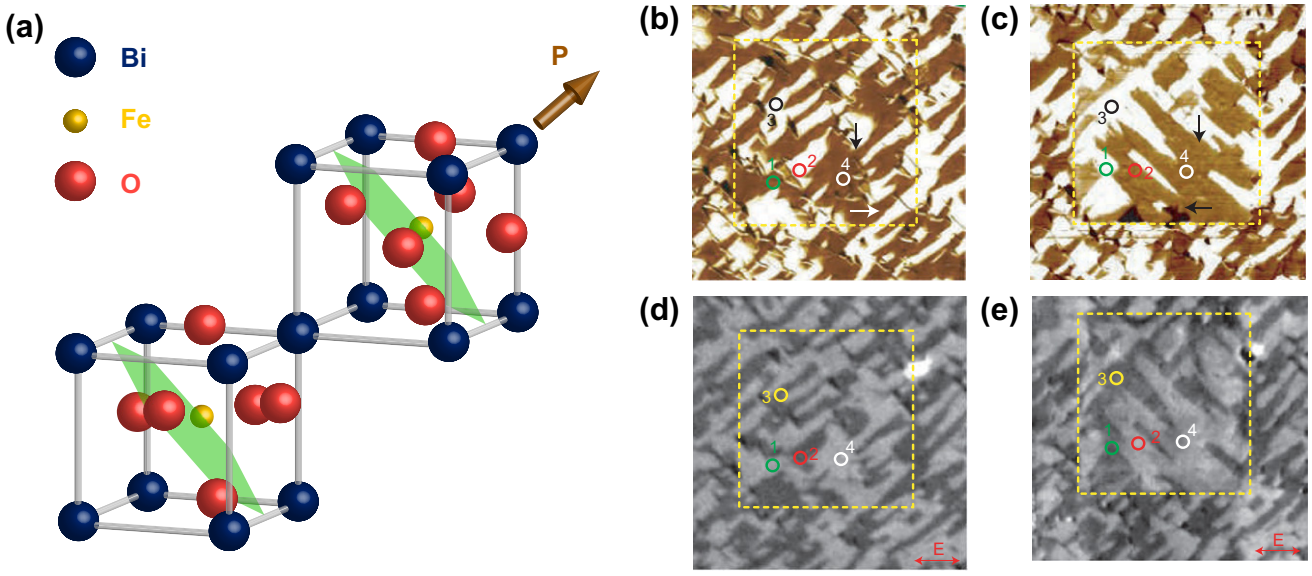

Fig. 5. Observation of antiferromagnetic domains in $BiFeO_3$ and their coupling to ferroelectric domains. (a) Schematic of two $BiFeO_3$ unit cells with opposite oxygen octahedral rotation. The antiferromagnetic easy plane (green plane) in bulk $BiFeO_3$ is always perpendicular to the ferroelectric polarization (brown arrow). (b and c) IP-PFM images showing the ferroelectric domain structure of $BiFeO_3/SrTiO_3$ film before and after the electrical switching, respectively, within the yellow rectangular area. (d and e) Corresponding XMLD-PEEM image of the same area before and after the electrical switching, which suggests that the antiferromagnetic domains always follow the ferroelectric domains.

(not shown), indicate that the domain structure of the BFO films is characterized by four polarization variants (i.e., circled areas in Fig. 5b).

Control of multiferroic behavior in BFO films relies on the ability of controlling the ferroelectric switching. To locally switch the polarization in the films, a DC bias is applied to the conducting atomic force microscope (AFM) tip while scanning over the desired area. By analyzing the OOP and IP contrast changes following this electrical poling, all three possible switching mechanisms (71°, 109°, and 180°) have been identified (Fig. 5c) [44].

The antiferromagnetic domain structure of BFO can be studied using PEEM based on XLD (Fig. 5d and e) [22,47]. Linear dichroism can arise from any anisotropy in charge distribution in a material. In non-ferroelectric antiferromagnets, such as $LaFeO_3$ discussed previously, the asymmetry of the electronic charge distribution due to magnetic order causes a difference in the absorption between orthogonal linear polarizations of light. This is manifested as a dichroism in X-ray absorption at the Fe $L_{3,2}$ edges, which can be used to distinguish different orientations of antiferromagnetic axis in domains. Non-magnetic ferroelectrics, such as PZT, also show linear dichroism because their polar-nature causes an asymmetric electronic charge distribution. Therefore, in BFO, both the antiferromagnetic and ferroelectric order can contribute to the dichroism. These two contributions can be separated by careful analysis of the temperature-dependence of the XLD and/or angle and polarization dependent measurements [22,47]. It was found that the antiferromagnetic and ferroelectric domains are intimately related and match up spatially. The combination of PFM and PEEM and the versatility of PEEM make these techniques ideal for the study of multiferroics.

The ability to control the nature of the ferroelectric switching in BFO offers an intriguing avenue by which we can study the coupling between ferroelectricity and antiferromagnetism in BFO films. Demonstration of room temperature magnetoelectric coupling is not only interesting from a fundamental point of view, but presents great potential for ultimately controlling magnetism with an applied electric field. To truly utilize such functionality for device applications, deterministic control of both antiferromagnetism and ferromagnetism is essential. To achieve such a goal, an approach has been proposed based on the presence of two distinct coupling mechanisms (Fig. 6a) [48]. The first is the coupling between ferroelectricity and antiferromagnetism in BFO as discussed earlier. It can be used to change the antiferromagnetic domain structure with an applied electric field. The second coupling mechanism of interest is based on a classic exchange coupling interaction [49] that arises at the interface between a ferromagnet and an antiferromagnet (Fig. 6a). Researchers have used such heterostructures to tune the properties of ferromagnets for over 50 years. With the addition of a multiferroic antiferromagnet, however, we now have the potential to control the state of the antiferromagnet electrically and thereby indirectly control the state of the ferromagnet by completing the bottom leg of the coupling triangle in Fig. 6a. Thus the combination of magnetoelectric coupling in a multiferroic and exchange coupling between magnetic materials offers a new pathway for the electrical control of ferromagnetism. Recently, several studies suggested the possibility of using such an approach to gain electrical control of a ferromagnet. Chu et al. have found that by using a combination of PFM and PEEM techniques, the coupling between a ferromagnetic CoFe layer and multiferroic BFO leads to a strong one-to-one correlation of their domain struc-

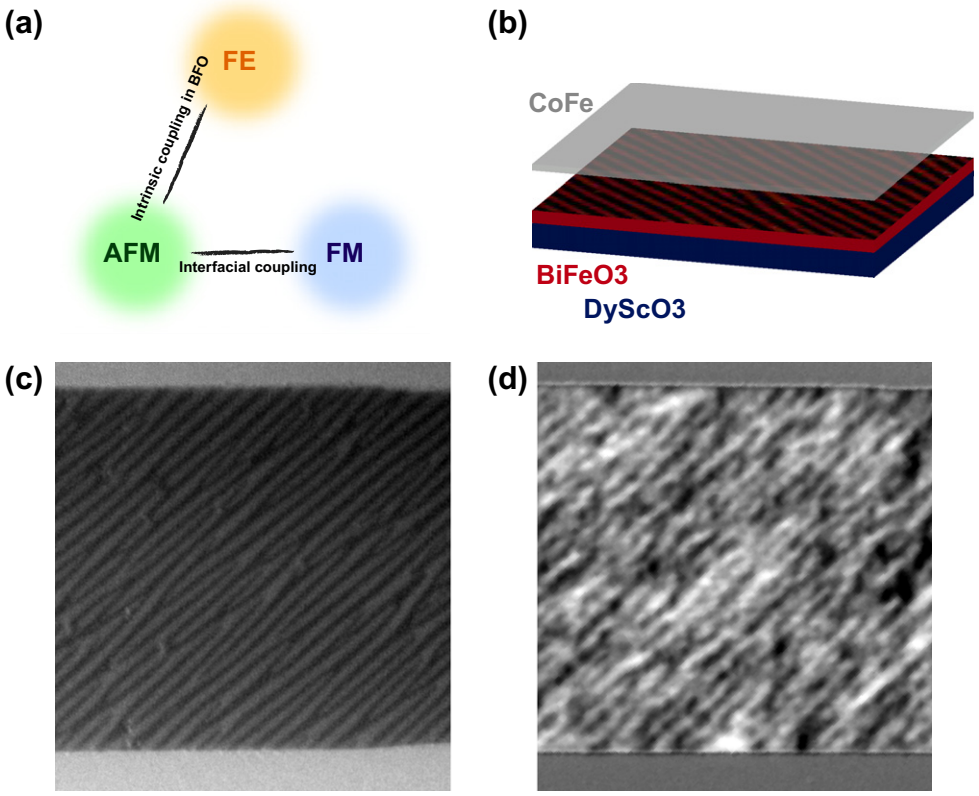

Fig. 6. Magnetoelectric coupling in a Pt(1.5 nm)/CoFe(2.5 nm)/$BiFeO_3$(100 nm)/$DyScO_3(001)_{pc}$ heterostructure. (a) Schematic of the coupling between the different order parameters in this system. The electric field control of ferromagnetism in CoFe is realized through the intrinsic coupling between ferroelectricity and antiferromagnetism in $BiFeO_3$, in combination with the interfacial coupling between the antiferromagnetic order in $BiFeO_3$ and the ferromagnetic order in CoFe. (b) Schematic of the heterostructure with the $BiFeO_3$ layer showing a 71° domain structure. (c) XMLD-PEEM image of $BiFeO_3$ showing antiferromagnetic domains. (d) XMCD-PEEM image taken at Co edge, in which the ferromagnetic domains are one-to-one correlated to the $BiFeO_3$ ferroelectric domains underneath.

tures [50]. When an electric field was applied in an in-plane test device structure, the 90° re-orientation of local magnetic moment was demonstrated. The same concept has also been shown to function using a BFO single crystal [51]. In the push for low-energy consumption memory and logic applications, establishing control of a magnetization reversal without the need of a magnetic field would be very advantageous.

In a recent study, the reversible and deterministic reversal of the ferromagnet's magnetization through the application of an electric field to the CoFe/BFO heterostructure, in absence of a magnetic field, was demonstrated at room temperature. In these experiments, PEEM was used to probe the interaction between ferromagnetic layer and BFO and to provide insights into the coupling mechanism. Based on those observations, a model has been proposed to explain the intriguing reversal mechanism. The robust, one-to-one magnetic coupling between a ferromagnetic layer and BFO causes the 180° reversal of the net magnetization of the ferromagnet in a device architecture. This observation is a milestone for the possible future use of multiferroics in room temperature, nonvolatile, and low-power consumption spintronics devices [52].

Another interesting example of multiferroic nanostructures is manifested in mixed phase BFO [53]. The concept originates from the ability to use epitaxial strain as a tool to create a new ground state of a material [54,55]. Large compressive epitaxial strains were imposed on the rhombohedral phase (R-phase) multiferroic, BFO which allows to stabilize the tetragonal-like phase (T-phase) with a significantly larger c/a ratio [56]. It was also demonstrated that partial relaxation of the epitaxial strain leads to the formation of a nanoscale mixture of the T- and R-phases, thus resembling a classical morphotropic phase boundary in modern piezoelectrics [57].

Partial strain relaxation through control of the film thickness leads to the formation of two orthogonal arrays of nanoscale, T + R phase mixtures, as imaged by AFM and shown in Fig. 7a. The individual stripe-like regions consist of a nanoscale ensemble of T- and R-phases with a characteristic length scale of 20–40 nm. XMCD-PEEM imaging has been used to explore the ferromagnetic response of BFO films with mixed phases, and compared to unconstrained R-and pure T-phase films [58]. X-ray absorption spectra at Fe^{3+} $L_{2,3}$-edge using left and right circularly polarized X-rays, at grazing incidence ($\theta = 30°$) were obtained as a function for different applied external magnetic fields. The significantly larger XMCD (~0.7%) spectra of mixed T + R phase BFO ensembles are observed, indicating that a higher magnetic moment is present in mixed phase BFO films. In order to explore the microscopic origins of this enhanced magnetic moment, the XMCD signal was imaged using PEEM. PEEM images were obtained using both LCP and RCP incident X-rays at a grazing incidence angle ($\theta = 30°$ to the sample surface). To enhance the difference in the magnetic contrast and eliminate the contribution from the topographic contrast, the ratio of the two images was taken. The image contrast is effectively a map of the local magnetization vector; regions that have their magnetic moment lying parallel to the X-ray wave vector appear bright, while those that are antiparallel appear dark. Fig. 7c is the PEEM image obtained by LCP X-ray, showing mainly topographic contrast. The darker areas in this image are in the recessed areas of the mixed phase features and brighter areas are elevated sections. The XMCD image, (Fig. 7d), reveals the intrinsic magnetic contrast that appears as bright and dark stripe-like pattern indicating that these stripes have magnetic moments lying parallel and antiparallel to the incident X-ray beam. By carefully determining the XMCD signal while rotating the sample with respect to the sample normal, the local magnetization direction of the stripes was found to be aligned along their long axis. Moreover, a series of temperature dependent XMCD-PEEM images show lower contrast level with elevated temperature (Fig. 7d–f), suggesting the existence of a magnetic phase transition at ~175 °C. It is worth noting that the XMCD contrast of the stripe features recovers when the sample is cooled down to room temperature.

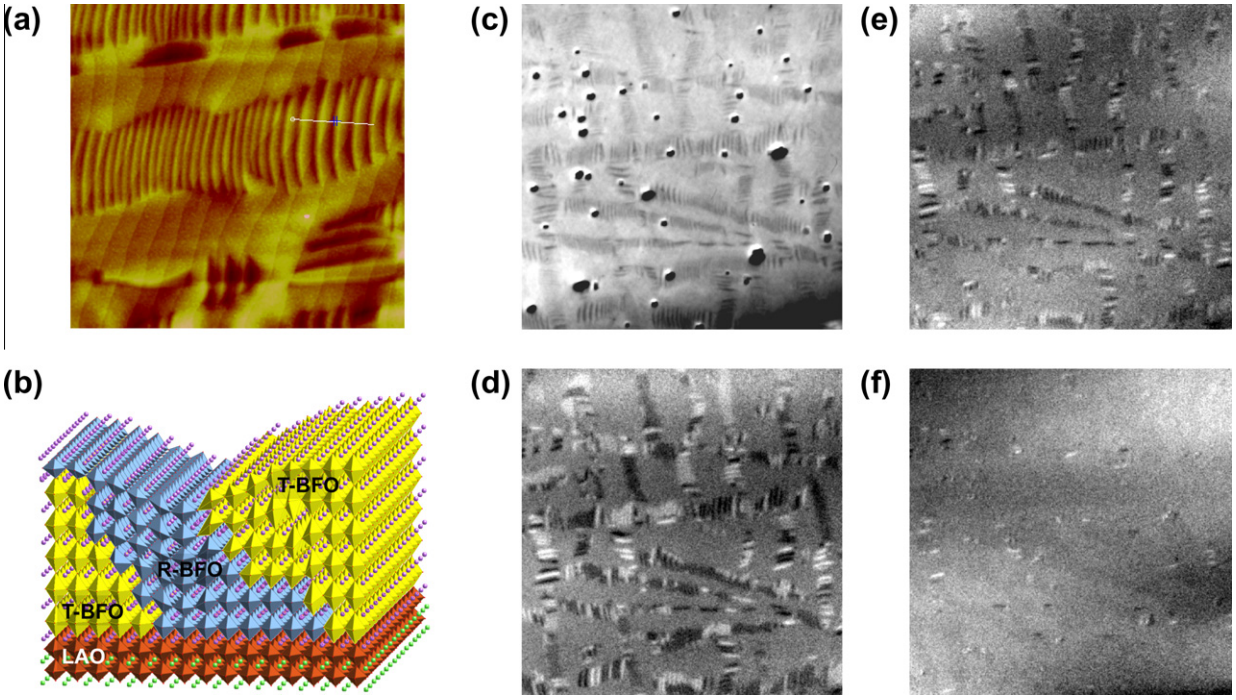

Fig. 7. Strain-induced magnetic phase in rhombohedral-tetragonal mixed phase $BiFeO_3$ films. (a) Typical topography image of mixed phase $BiFeO_3$ films taken with atomic force microscope. The stripe-like areas in this image are where the rhombohedral and tetragonal phases co-exist. (b) Schematic of mixed phase $BiFeO_3$ at cross-sectional view. The highly distorted rhombohedral phase is constraint by the tetragonal phase. (c) PEEM image showing mainly topography of the film. (d–f) XMCD-PEEM image at various temperatures (room temperature, 125 °C, and 175 °C, respectively). The highly distorted rhombohedral phase has strong magnetic response to the circularly polarized X-rays; a magnetic transition can be observed at ~175 °C.

By careful analysis on PEEM and PFM images, we found the highly distorted R-phase, constrained between the T-phases (as schematically illustrated in Fig. 7b), to be the source of the enhanced magnetic moment in the XMCD image, arising from a piezomagnetic effect [59,60]. That the nanoscale magnetic moment in the highly distorted R-phase can be controlled by an electric field has been also demonstrated. The magnetic moments in these stripe-shaped nanoscale mixed phase regions can be erased and rewritten at room temperature with only the application of an electric field.

6. Outlook

Several challenges remain in multiferroic research, and PEEM will keep serving as an important characterization tool providing critical information to understand the fundamental science. For instance, in order to push the ferromagnet/multiferroic heterostructures into the real device applications, several key issues need to be addressed, such as power consumption, switching speed, the scalability. Especially for scale-down issue, nano-size device needs to be constructed, the competition between coupling of ferromagnet/multiferroic and coupling between individual ferromagnetic nano-dots are essential information determining the device size. PEEM can be used to probe the local coupling of these nano-devices (Fig. 8a) [61]. Single-phase multiferroics with spontaneous and simultaneous ferroelectric and ferromagnetic order at ambient conditions still remain elusive. Many studies have aimed on site-engineering by ionic substitutions to enhance the magnetic properties in proper ferroelectrics [62]. PEEM can be served as a critical tool to understand the mutual coupling between the substitution and original Fe ions and provide new insights for designing multiferroic materials. Another approach to create magnetoelectric multiferroic is using self-assembled nano-composite materials (Fig. 8b) [63,64], i.e. a combination of immiscible perovskite, BFO, and spinel, $CoFe_2O_4$. The strong piezoelectricity of BFO and remarkable magnetostriction of $CoFe_2O_4$ was expected to provide a strong if indirect coupling of the two materials [65]. Several studies suggested the strong coupling in this system and demonstrated the ability to electrical switch $CoFe_2O_4$ nano-pillars with a small magnetic field [66]. However, magnetic coupling has not been reported yet. The key questions to be answered is the magnetic coupling between matrix BFO and nano $CoFe_2O_4$ pillars and the magnetic coupling mediated by stray filed between pillars. PEEM will be a power tool to obtain detailed information to address these questions [67].

Interfaces have emerged as key focal points of current condensed matter science [68,69]. In complex, correlated oxides, heterointerfaces provide a powerful route to create and manipulate the charge, spin, orbital, and lattice degrees of freedom. The interaction of degrees of freedom at the interface has resulted in a number of exciting discoveries including the observation of a 2-D electron gas-like behavior at $LaAlO_3$–$SrTiO_3$ interfaces; [70] the emergence of the ferromagnetism in a superconducting material at a $YBa_2Cu_3O_{7-x}$–$La_{0.7}Ca_{0.3}MnO_3$ interface [71] and a ferromagnetic state induced in a $BiFeO_3$ layer at a heterointerface with $La_{0.7}Sr_{0.3}MnO_3$ (Fig. 8c) [72]. PEEM studies on interface systems have provided orbital (XMLD) and spin (XMCD) information to understand the intriguing phenomena observed in these systems with spatial resolution. Temperature dependent measurements can provide more details on the coupling strength. In ferroic oxides, such as ferroelectrics, domain walls emerge as natural interfaces as a consequence of the minimization of electrostatic and elastic energies. Recently, several key studies pointed out interesting observations on domain walls in multiferroics, for example in BFO systems 109° domain walls have been suggested to be the origin of the exchange bias in ferromagnet/BFO heterostructures, which suggests these domain walls might be magnetic (Fig. 8d) [73,74]. XAS-XMCD spectroscopy has been applied to show enhanced XMCD response in 109° domain walls samples [74]. However, the magnetic characterization with spatial resolution and element sensitivity is needed to provide local information to address the magnetism at domain walls. This approach can be extended to study other related topological defects in strongly correlated systems.

In the study of the intriguing physics in multiferroics, PEEM has been extensively used as a key technique to investigate multiple order parameters individually, as well as the coupling between

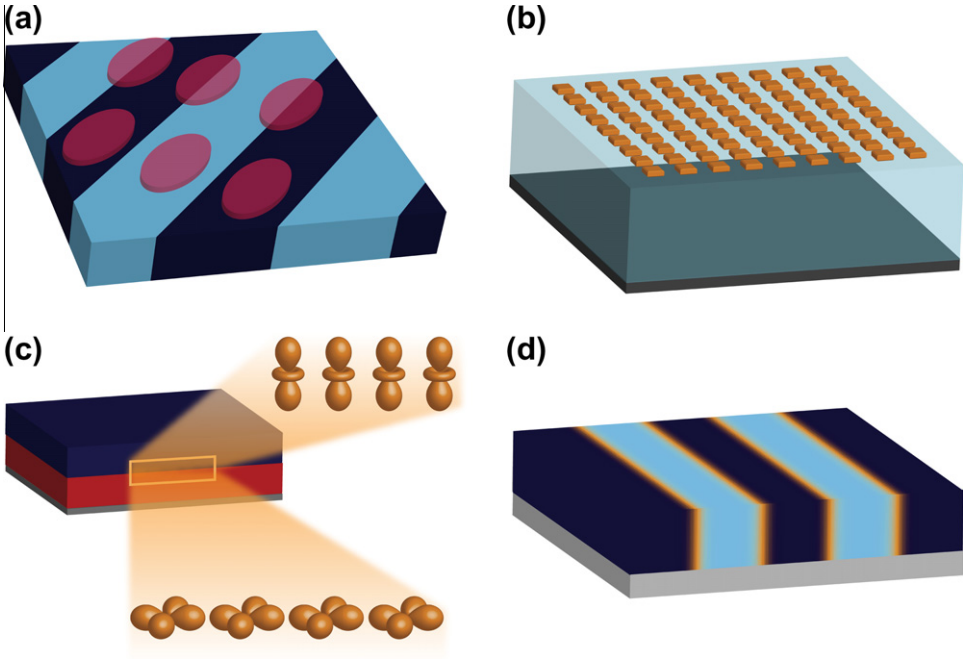

Fig. 8. Multiferroic nanostructures of interest. (a) Patterned nano-scale ferromagnetic/multiferroic devices. (b) Self-assembled vertical nano-structure. (c) Interface induced orbital/spin reconstruction. (d) Domain walls in multiferroics.

them. Its nano-scale spatial resolution allows us to look closer into one single domain where the emergent phenomena can be studied locally in these complex systems.

Acknowledgments

The authors acknowledge the support of the Director, Office of Basic Energy Sciences, Materials Science Division of the US Department of Energy under Contract No. DE-AC02-05CH11231 and previous contracts, ONR-MURI under Grant No. E21-6RU-G4 and previous contracts, and the Western Institute of Nanoelectronics program as well as significant intellectual and financial support from scientists and engineers at Intel. Over the past 8–10 years, R.R. has also benefitted significantly through funding from the Office of Naval Research (through a MURI program from 2003–2008) as well as funding from the National Science Foundation during his tenure at the University of Maryland, College Park.

References

[1] Spaldin NA, Cheong SW, Ramesh R. Multiferroics: Past, present, and future. Phys Today 2010;63:38–43.
[2] Spaldin NA, Fiebig M. The renaissance of magnetoelectric multiferroics. Science 2005;309:391–2.
[3] Cheong SW, Mostovoy M. Multiferroics: a magnetic twist for ferroelectricity. Nature Mater 2007;6:13–20.
[4] Eerenstein W, Mathur ND, Scott JF. Multiferroic and magnetoelectric materials. Nature 2006;442:759–65.
[5] Ramesh R, Spaldin NA. Multiferroics: progress and prospects in thin films. Nature Mater 2007;6:21–9.
[6] Martin LW, Chu YH, Ramesh R. Advances in the growth and characterization of magnetic, ferroelectric, and multiferroic oxide thin films. Mater Sci Eng R 2010;68:111–33.
[7] Lee S, Pirogov A, Kang M, Jang KH, Yonemura M, Kamiyama T, et al. Giant magneto-elastic coupling in multiferroic hexagonal manganites. Nature 2008;451:805–9.
[8] Ko KT, Jung MH, He Q, Lee JH, Woo CS, Chu K, et al. Concurrent transition of ferroelectric and magnetic ordering near room temperature. Nature Commun 2012;2:567.
[9] Liu HJ, Liang CW, Liang WI, Chen HJ, Yang JC, Peng CY, et al. Strain-driven phase boundaries in $BiFeO_3$ thin films studied by atomic force microscopy and X-ray diffraction. Phys Rev B 2012;85:014104.
[10] Lebeugle D, Colson D, Forget A, Viret M, Baraille AM, Gukasov A. Electric-field-induced spin flop in $BiFeO_3$ single crystals at room temperature. Phys Rev Lett 2008;100:227602.
[11] Lottermoser T, Meier D, Pisarev RV, Fiebig M. Giant coupling of second-harmonic generation to a multiferroic polarization. Phys Rev B 2009;80:100101.
[12] Ravillain P, de Sousa R, Gallais Y, Sacuto A, Measson MA, Colson D, et al. Electric-field control of spin waves at room temperature in multiferroic $BiFeO_3$. Nature Mater 1987;12:975–9.
[13] Choi T, Horibe Y, Yi HT, Choi YJ, Wu W, Cheong SW. Insulating interlocked ferroelectric and structural antiphase domain walls in multiferroic. Nature Mater 2010;9:253–8.
[14] Chu YH, Cruz MP, Yang CH, Martin LW, Yang PL, Zhang JX, et al. Domain control in multiferroic $BiFeO_3$ through substrate vicinality. Adv Mater 2007;19:2662–6.
[15] Spaldin NA. Magnetic materials: fundamentals and applications. 2nd ed. Cambridge University Press; 2010.
[16] Kittel C. Introduction to solid state physics. 8th ed. John Wiley & Sons Inc.; 2005.
[17] Fiebig M, Lottermoser T, Frohlich D, Goltsev AV, Pisarev RV. Observation of coupled magnetic and electric domains. Nature 2002;419:818–20.
[18] Anders S, Padmore HA, Duarte RM, Renner T, Stammler T, Scholl A, et al. Photoemission electron microscope for the study of magnetic materials. Rev Sci Instrum 1999;70:3973–81.
[19] Stöhr J, Padmore HA, Anders S, Stammler T, Scheinfein MR. Principles of X-ray magnetic dichroism spectromicoscopy. Surf Rev Lett 1998;5:1297–308.
[20] Stöhr J. NEXAFS spectroscopy. Springer; 1996.
[21] Stöhr J, Siegman HC. Magnetism. Springer; 2006.
[22] Zhao T, Scholl A, Zavaliche F, Lee K, Barry M, Doran A, et al. Electrical control of antiferromagnetic domains in multiferroic $BiFeO_3$ films at room temperature. Nature Mater 2006;5:823–9.
[23] Wu J, Choi J, Scholl A, Doran A, Arenholz E, Wu YZ, et al. Element-specific study of the anomalous magnetic interlayer coupling across NiO spacer layer in Co/NiO/Fe/Ag(001) using XMCD and XMLD. Phys Rev B 2009;80:012409.
[24] Metzler R, Zhou D, Coppersmith S, Scholl A, Doran A, Young A, et al. Gradual ordering in red abalone nacre. J Am Chem Soc 2008;130:17519–27.
[25] Choe SB, Acremann Y, Scholl A, Bauer A, Doran A, Stöhr J, et al. Vortex-driven magnetization dynamics. Science 2004;304:420–2.
[26] Dawber M, Rabe KM, Scott JF. Physics of thin-film ferroelectric oxides. Rev Mod Phys 2005;77:1083–130.
[27] Scott JF, Paz de Araujo CA. Ferroelectric memories. Science 1989;246:1400–5.
[28] Arenholz E, van der Laan G, Fraile-Rodríguez A, Yu P, He Q, Ramesh R. Probing ferroelectricity in $PbZr_{0.2}Ti_{0.8}O_3$ with polarized soft X-rays. Phys Rev B 2010;82:140103(R).
[29] Ganpule CS, Nagarajan V, Hill BK, Roytburd AL, Williams ED, Ramesh R, et al. Imaging three-dimensional polarization in epitaxial polydomain ferroelectric thin films. J Appl Phys 2002;91:1477–81.
[30] Baruchel J. X-ray and neutron topographical studies of magnetic-materials. Physica B 1993;192:79–93.
[31] Scholl A, Stöhr J, Lüning J, Seo JW, Fompeyrine J, Siegwart H, et al. Observation of antiferromagnetic domains in epitaxial thin films. Science 2000;287:1014–6.
[32] Kuiper P, Searle BG, Rudolf P, Tjeng LH, Chen CT. X-ray magnetic dichroism of antiferromagnet Fe_2O_3: The orientation of magnetic moments observed by Fe 2*p* X-ray absorption spectroscopy. Phys Rev Lett 1993;70:1549–52.
[33] Stöhr J, Scholl A, Regan TJ, Anders S, Lüning J, Scheinfein MR, et al. Images of the antiferromagnetic structure of a NiO(100) surface by means of X-ray magnetic linear dichroism spectromicroscopy. Phys Rev Lett 1999;83:1862–3.
[34] Alders D, Tjeng LH, Voogt FC, Hibma T, Sawatzky GA, Chen CT, et al. Temperature and thickness dependence of magnetic moments in NiO epitaxial films. Phys Rev B 1998;57:11623–31.
[35] Thole BT, van der Laan G, Sawatzky GA. Strong magnetic dichroism predicted in the $M_{4,5}$ X-ray absorption spectra of magnetic rare-earth materials. Phys Rev Lett 1985;55:2086–8.
[36] Khomskii DI. Multiferroics: different ways to combine magnetism and ferroelectricity. J Mag Mag Mater 2006;306:1–8.
[37] Wang J, Neaton JB, Zheng H, Nagarajan V, Ogale SB, Liu B, et al. Epitaxial $BiFeO_3$ multiferroic thin film heterostructures. Science 2003;299:1719–22.
[38] Huang ZJ, Cao Y, Sun YY, Xue YY, Chu CW. Coupling between the ferroelectric and antiferromagnetic orders in $YMnO_3$. Phys Rev B 1997;56:2623–6.
[39] Subramanian MA, He T, Chen JZ, Rogado NS, Calvarese TG, Sleight AW. Giant room-temperature magnetodielectric response in the electronic ferroelectric $LuFe_2O_4$. Adv Mater 2006;18:1737–41.
[40] Kimura T, Goto T, Shintani H, Ishizaka K, Arima T, Tokura Y. Magnetic control of ferroelectric polarization. Nature 2003;426:55–8.
[41] Hur N, Park S, Sharma PA, Ahn JS, Guha S, Cheong SW. Electric polarization reversal and memory in a multiferroic material induced by magnetic fields. Nature 2004;429:392–5.
[42] Catalan G, Scott JF. Physics and applications of bismuth ferrite. Adv Mater 2009;21:2463–85.
[43] Kubel F, Schmid H. Structure of a ferroelectric and ferroelastic monodomain crystal of the perovskite $BiFeO_3$. Acta Cryst 1990;B46:698–702.
[44] Zavaliche F, Yang SY, Zhao T, Chu YH, Cruz MP, Eom CB, et al. Multiferroic $BiFeO_3$ films: domain structure and polarization dynamics. Phase Trans 2006;79:991–1017.
[45] Neaton JB, Ederer C, Waghmare UV, Spaldin NA, Rabe KM. First-principles study of spontaneous polarization in multiferroic $BiFeO_3$. Phys Rev B 2005;71:014113.
[46] Ederer C, Spaldin NA. Weak ferromagnetism and magnetoelectric coupling in bismuth ferrite. Phys Rev B 2005;71:060401.
[47] Holcomb MB, Martin LW, Scholl A, He Q, Yu P, Yang CH, et al. Probing the evolution of antiferrmagnetism in multiferroics. Phys Rev B 2010;81:134406.
[48] Chu YH, Martin LW, Holcomb MB, Ramesh R. Controlling magnetism with multiferroics. Mater Today 2007;10:16–23.
[49] Nogues J, Schuller IK. Exchange bias. J Mag Mag Mater 1999;192:203–32.
[50] Chu YH, Martin LW, Holcomb MB, Gajek M, Han SJ, He Q, et al. Electric-field control of local ferromagnetism using a magnetoelectric multiferroic. Nature Mater 2008;7:478–82.
[51] Lebeugle D, Mougin A, Viret M, Colson D, Ranno L. Electric field switching of the magnetic anisotropy of a ferromagnetic layer exchange coupled to the multiferroic compound $BiFeO_3$. Phys Rev Lett 2009;103:257601.
[52] Heron JT, Trassin M, Ashraf K, Gajek M, He Q, Yang SY, et al. Electric-field-induced magnetization reversal in a ferromagnet-multiferroic heterostructure. Phys Rev Lett 2011;107:217202.
[53] Zeches RJ, Rossell MD, Zhang JX, Hatt AJ, He Q, Yang CH, et al. A strain-driven morphotropic phase boundary in $BiFeO_3$. Science 2009;326:977–80.
[54] Haeni JH, Irvin P, Chang W, Uecker R, Reiche P, Li YL, et al. Room-temperature ferroelectricity in strained $SrTiO_3$. Nature 2004;430:758–61.
[55] Choi KJ, Biegalski M, Li YL, Sharan A, Schubert J, Uecker R, et al. Enhancement of ferroelectricity in strained $BaTiO_3$ thin films. Science 2004;306:1005–9.
[56] Damodaran AR, Liang CW, He Q, Peng CY, Chang L, Chu YH, et al. Nanoscale structure and mechanism for enhanced electromechanical response of highly strained $BiFeO_3$ thin films. Adv Mater 2011;23:3170–5.
[57] Zhang JX, Xiang B, He Q, Seidel J, Zeches RJ, Yu P, et al. Large field-induced strains in a lead-free piezoelectric material. Nature Nanotechnol 2011;6:98–102.
[58] He Q, Chu YH, Heron JT, Yang SY, Laing WI, Kuo CY, et al. Electrically controllable spontaneous magnetism in nanoscale mixed phase multiferroics. Nature Commun 2011;2:225.
[59] Moriya T. Anisotropic superexchange interaction and weak ferromagnetism. Phys Rev 1960;120:91–6.
[60] Philips TG, Townsend Jr RL, White RL. Piezomagnetism of CoF_2 and α-Fe_2O_3 from electron-paramagnetic-resonance pressure experiments. Phys Rev Lett 1967;18:646–7.

[61] Wu J, Carlton D, Park JS, Meng Y, Arenholz E, Doran A. Direct observation of imprinted antiferromagnetic vortex states in CoO/Fe/Ag(001) discs. Nature Phys 2011;7:303–6.
[62] Nechache R, Harnagea C, Pignolet A, Normandin F, Veres T, Carignan LP, et al. Growth, structure, and properties of epitaxial thin films of first-principles predicted multiferroic Bi_2FeCrO_6. Appl Phys Lett 2006;89:102902.
[63] Zheng H, Wang J, Lofland SE, Ma Z, Mohaddes-Ardabili L, Zhao T, et al. Multiferroic $BaTiO_3$-$CoFe_2O_4$ nanostructures. Science 2004;303:661–3.
[64] Nan CW, Bichurin MI, Dong SX, Viehland, Srinivasan G. Multiferroic magnetoelectric composites: historical perspective, status, and future directions. J Appl Phys 2008;103:031101.
[65] Zheng H, Straub F, Zhan Q, Yang PL, Hsieh WK, Zavaliche F, et al. Self-assembled growth of $BiFeO_3$–$CoFe_2O_4$ nanostructures. Adv Mater 2006;18:2747–52.
[66] Zavaliche F, Zhao T, Zheng H, Straub F, Cruz MP, Yang PL, et al. Electrically assisted magnetic recording in multiferroic nanostructures. Nano Lett 2007;7:1586–90.
[67] Zhao T, Scholl A, Zavaliche F, Zheng H, Barry M, Doran A, et al. Nanoscale X-ray magnetic circular dichroism probing of electric-field-induced magnetic switching in multiferroic nanostructures. Appl Phys Lett 2007;90:123104.
[68] Takagi H, Hwang HY. An emergent change of phase for electronics. Science 2010;327:1601–2.
[69] Mannhart J, Schlom DG. Oxide interfaces – an opportunity for electronics. Science 2010;327:1607–11.
[70] Ohtomo A, Hwang HY. A high-mobility electron gas at the $LaAlO_3/SrTiO_3$ heterointerface. Nature 2004;427:423–6.
[71] Chakhalian J, Freeland JW, Srajer G, Strempfer J, Khaliullin G, Cezar JC, et al. Magnetism at the interface between ferromagnetic and superconducting oxides. Nature Phys 2006;2:244–8.
[72] Yu P, Lee JS, Okamoto S, Rossell MD, Huijben M, Yang CH, et al. Interface ferromagnetism and orbital reconstruction in $BiFeO_3$–$La_{0.7}Sr_{0.3}MnO_3$ heterostructures. Phys Rev Lett 2010;105:027201.
[73] Bea H, Bibes M, Ott F, Dupe B, Zhu XH, Petit S, et al. Mechanisms of exchange bias with multiferroic $BiFeO_3$ epitaxial thin films. Phys Rev Lett 2008;100:017204.
[74] Martin LW, Chu YH, Holcomb MB, Huijben M, Yu P, Han SJ, et al. Nanoscale control of exchange bias with $BiFeO_3$ thin films. Nano Lett 2008;7:2050–5.